HAL open science

On Damping Rates of dissipative KdV equations

Jean-Paul Chehab, Georges Sadaka

▶ To cite this version:

Jean-Paul Chehab, Georges Sadaka. On Damping Rates of dissipative KdV equations. 2012. hal-00734292

HAL Id: hal-00734292

https://hal.science/hal-00734292v1

Submitted on 8 Oct 2012

HAL is a multi-disciplinary open access archive for the deposit and dissemination of scientific research documents, whether they are published or not. The documents may come from teaching and research institutions in France or abroad, or from public or private research centers.

L'archive ouverte pluridisciplinaire **HAL**, est destinée au dépôt et à la diffusion de documents scientifiques de niveau recherche, publiés ou non, émanant des établissements d'enseignement et de recherche français ou étrangers, des laboratoires publics ou privés.

On Damping Rates of dissipative KdV equations

Jean-Paul Chehab

LAMFA, UMR 7352, Université de Picardie Jules Verne
Pôle Scientifique, 33, rue Saint Leu, 80039 Amiens, France
and
Projet SIMPAF, INRIA Nord-Europe

Georges Sadaka [1]

LAMFA, UMR 7352, Université de Picardie Jules Verne
Pôle Scientifique, 33, rue Saint Leu, 80039 Amiens, France

Abstract : We consider here different models of dissipative Korteweg-de Vries (KdV) equations on the torus. Using a proper wave function Γ, we compare numerically the long time behavior effects of the damping models and we propose a hierarchy between these models. We also introduce a method based on the solution of an inverse problem to rebuild *a posteriori* the damping operator using only samples of the solution.

1 Introduction

The modeling and the underlying mathematical analysis of gravity waves is still a challenging topic despite intensive works and progress that have been done, especially during the last decade, see, e.g. [22] for the derivation of the models. The long time behavior of dissipative asymptotic models remains an important issue: capturing damping rates in several norms, measuring regularization effect or pointing out complex asymptotic dynamics (existence of attractors, Hopf bifurcations etc) to name but a few are important points for the understanding of natural phenomena. For many models, several of these questions are still open and the numerical simulation is a way to capture some properties and to select pertinent models.

Damped Korteweg-de Vries equations (KdV) appear in different physical situations and they can be expressed in a large generality on the torus $\mathbb{T} = \mathbb{T}(0, L)$ as

$$u_t + \mathcal{L}(u) + u_{xxx} + uu_x = 0, x \in \mathbb{T},\ t > 0, \tag{1}$$

where $\mathcal{L}$ is a linear operator, defined on a Hilbert space V, subspace of L^2 and satisfying

$$\int_0^L \mathcal{L}(v)vdx \geq 0, \tag{2}$$

for all function $v \in V$, regular enough, in such a way the L^2-norm of the solution is decreasing in time as

$$\frac{1}{2}\frac{d|u|^2_{L^2}}{dt} + \int_0^L \mathcal{L}(v)vdx = 0. \tag{3}$$

1. The second author is supported by the program "appui à l'émergence" of the Région Picardie

The definition of $\mathcal{L}$ depends on the physical situations: in [23], Ott and Sudan have proposed a damped KdV equation as a model of Landau damping for ion acoustic wave, the (linear) damping being nonlocal, and in [24] they have presented different models of damping taking $\mathcal{L}(u) = |D|^\alpha u$, where $|D| = \sqrt{-\Delta}$; in [5] Dias and Dutykh have considered the operators

$$\mathcal{L}(u) = -\nu u_{xx} + \sqrt{\frac{\nu}{2}} \int_0^t \frac{u_t(s)}{\sqrt{t-s}} ds, \tag{4}$$

$$\mathcal{L}(u) = -\nu u_{xx} - \sqrt{\frac{\nu}{2}} \int_0^t \frac{u_x(s)}{\sqrt{t-s}} ds, \tag{5}$$

respectively, to model natural damping of water waves, mathematical analysis and simulations can be found also in [2, 4, 10]; in [3, 26] it has been proposed a general model of weak damping for spatial nonlocal frequency by frequency damping,

$$\mathcal{L}(u) = \sum_{k \in \mathbb{Z}} \gamma_k \hat{u}_k e^{\frac{2i\pi kx}{L}}. \tag{6}$$

Generally, we do not have damping rate estimates so it is difficult to make a hierarchy between these models without using numerical simulations. We are here interested in comparing the long time effect of these different type of damping and for that purpose, we follow [3] using the norm ratio function

$$\Gamma(t; u) = \frac{\sqrt{< \mathcal{L}(u), u >}}{|u|},$$

that allows to compare the damping in L^2 norm; here $|.|$ and $< ., . >$ denote respectively the L^2-norm and the associated scalar product. A consequence of relation is that the L^2 decay depends on $\mathcal{L}$, in fact an application of a Gronwall lemma gives

$$|u(t)|^2 = e^{-2\int_0^t \Gamma^2(s) ds} |u(0)|^2. \tag{7}$$

so that Γ characterizes the damping in L^2.

A interesting inverse problem is the following: starting from samples of u at discrete times t_m that can be measured (u represents the vertical elevation of the wave with respect to the horizontal position), is it possible to rebuild a given type of damping operator whose the effect on large time interval fits with $\Gamma^2(t)$?

The present work addresses to these two questions and we propose some numerical techniques that allow in the one hand, to compare the effect of different damping models on large time interval and, on the other hand, starting from samples of the solution, to recover numerically an approximation of the operator $\mathcal{L}$.

The article is organized as follows: in Section 2 we recall some damping properties of the different models and we introduce the tools that we will use for making the hierarchy. After that, in Section 3, we present the numerical schemes in space and in time. Then, in Section 4, we first compare numerically the long time behavior of the damping and we display a time signal analysis of $\Gamma(t)$. After that, we propose to rebuild in some cases and *a posteriori* the damping operator by fitting proper parameters with the solution of a constraint least square problem.

2 Damping properties

2.1 The different models

We here recall some characteristics and properties of the damping we will consider for the application.

2.1.1 Weakly damped KdV equations

Consider the situation in which the damping operator can be described by Fourier series as

$$\mathcal{L}(u) = \sum_{k\in\mathbb{Z}} \gamma_k \hat{u}_k e^{\frac{2i\pi kx}{L}},$$

where $\gamma_k \geq 0$ are the damping weights and $\hat{u}_k$ denotes the k-th Fourier coefficient of u ; the assumption of positivity of γ_k implies that

$$< \mathcal{L}(u), u >= \sum_{k\in\mathbb{Z}} \gamma_k \hat{u}_k^2 \geq 0,$$

insuring the decreasing in time of the L^2-norm of the solution. The choice $\gamma_k = \left|\frac{2\pi k}{L}\right|^\alpha, \alpha > 0$ corresponds to $\mathcal{L}_\gamma(u) = |D|^\alpha u$, where $|D| = \sqrt{-\Delta}$. More generally, when $\lim_{k\to+\infty} \gamma_k = +\infty$, (e.g. $\gamma_k = k^2$ for a parabolic damping [11]), the equation is regularizing at finite time. When γ_k is constant, say $\mathcal{L}(u) = \gamma u$, the damping is said to be "weak" and is not regularizing at finite time but, as proved by Ghidaglia [12, 13] and Goubet [14, 15], it allows the equation to have a finite dimensional attractor which is in a more regular space than the initial data: this is the asymptotic regularization property. In all these situations $\gamma_k \geq \gamma > 0$ is bounded from below and the damping in L^2-norm is done at least at an exponential rate, we have indeed, after integration by parts and use of Gronwall's lemma,

$$\|u\|_{L^2} \leq e^{-\gamma t}\|u_0\|_{L^2}.$$

In [3], the limit case, ($\lim_{k\to+\infty} \gamma_k = 0$) has been considered, and it was pointed out numerically also asymptotic regularization properties but the damping rate is not uniform: it depends on both the sequence γ and of the Fourier coefficients of the initial data, see [3].

2.1.2 Nonlocal damping in time

The nonlocal damping in time

$$\mathcal{L}(u)(x,t) = -\nu u_{xx} - \frac{\sqrt{\nu}}{\sqrt{\pi}}\int_0^t \frac{u_t(s)}{\sqrt{t-s}}ds.$$

was considered by Dias and Dutykh in [5]. The associated Damped KdV equation

$$u_t + u_{xxx} + uu_x - \nu u_{xx} - \frac{\sqrt{\nu}}{\sqrt{\pi}}\int_0^t \frac{u_t(s)}{\sqrt{t-s}}ds = 0 \tag{8}$$

models one way water waves in a fluid layer of finite depth under the influence of viscous effects.
A model of the same kind is studied in [1, 5], say

$$u_t + u_{xxx} + uu_x - \nu u_{xx} - \frac{\sqrt{\nu}}{\sqrt{\pi}}\int_0^t \frac{u_x(s)}{\sqrt{t-s}}ds = 0 \tag{9}$$

but it will not considered in the present work. A mathematical analysis is presented in [4] a numerical study is realized in [10].

2.1.3 Localized damping in space

It corresponds to

$$\mathcal{L}(u)(x,t) = \chi_{[a,b]}u,$$

where $0 < a < b < L$. This situation have been considered in the context of the stabilization of KdV equations, when the domain is the torus $\mathbb{T}$ [20] or the half line $\mathbb{R}^+$ and $\mathcal{L} = \chi_{[a_0,+\infty[}$ with $a_0 > 0$, [25]. A exponential decay in time was established in proper Sobolev norms. We will recover numerically on $\mathbb{T}$ this exponential rate of convergence (after a transient time) and compare it to the other damping models, see Section 4.

2.2 Comparison of the damping

As stated in the introduction, we would like to compare numerically these damping models for long time intervals and to display a time signal analysis. This is a first step to be considered for making a hierarchy. To this end, we follow [3] and introduce the function $\Gamma(t)$

$$\Gamma(u)(t) = \sqrt{\frac{< \mathcal{L}(u), u >}{< u, u >}}, \tag{10}$$

that we will note $\Gamma(t)$ for simplicity. In the general case, we can prove that $|u|_{L^2} \to 0$ as $t \to +\infty$ but without deriving explicit bounds for the damping rate:

Proposition 1. *Assume that*
– $\mathcal{L} : V \subset L^2 \to L^2$ *is linear continuous*
– $< \mathcal{L}(u), u > \geq 0$
– $< \mathcal{L}(u), u >= 0 \Longrightarrow u = 0$
then $\lim\limits_{t\to+\infty} |u|_{L^2} = 0$.

Proof. By taking the scalar product in L^2 of the equation with u, we obtain after an integration by parts

$$\frac{1}{2}\frac{d|u|^2}{dt} + < \mathcal{L}(u), u >= 0, \tag{11}$$

making the function $t \mapsto |u|$ decreasing in time. Assuming that u is smooth enough and arguing that $|u| \geq 0$ we deduce that $|u|$ converges towards a limit ℓ as t goes to ∞. This implies that $< \mathcal{L}(u), u > \to 0$ as t goes to $+\infty$, hence that $u \to 0$ a.e. □

The function $\Gamma(t)$ is related to the L^2 norm of the solution: we recall the simple Gronwall lemma from [3]

Proposition 2. *Let $u(x,t)$ be a regular solution of equation (1). We assume that $G(u,t)$ is $\mathcal{C}^1$ in t. Then we have the relation*

$$|u(t)|^2_{L^2} = e^{-\int_0^t \Gamma^2(s)ds}|u_0|^2_{L^2}.$$

In particular, $\lim\limits_{t\to+\infty} |u|_{L^2} = 0$ *iff* $t \mapsto G(t) \notin L^2_t(0,+\infty)$.

Of course, the damping rate in L^2 depends on the operator $\mathcal{L}$, so it appears that the function $\Gamma(t)$ is an appropriate tool for comparing two damping in long time intervals.
For these reasons, we propose in section 4 to provide a time signal analysis using a proper orthogonal polynomial basis associated to a weighted L^2 scalar product.

Let us consider u and v respectively (regular) solutions of the damped KdV equations

$$u_t + \mathcal{L}_1(u) + u_{xxx} + uu_x = 0, x \in \mathbb{T},\ t > 0,$$

and

$$v_t + \mathcal{L}_2(v) + v_{xxx} + vvx = 0, x \in \mathbb{T},\ t > 0.$$

We let $w = u_1 - u_2$. We can write

$$w_t + w_{xxx} + \mathcal{L}_1(w) + (\mathcal{L}_1 - \mathcal{L}_2)(v) + ww_x + wv_x + vw_x = 0.$$

Then, taking the L^2- scalar product of these terms with w, we obtain after the usual simplifications,

$$\frac{1}{2}\frac{d|w|^2}{dt} + < \mathcal{L}_1(w), w > + \frac{1}{2}\int_0^L w^2 v_x dx + < (\mathcal{L}_1 - \mathcal{L}_2)(v), w >= 0.$$

The comparison of two solutions generated by two different damped KdV models needs to make additional assumption. It is however possible to make a comparison in the case of weak damping, i.e. when $\mathcal{L}$ is defined as

$$\mathcal{L}(u) = \mathcal{L}_\gamma(u) = \sum_{k\in\mathbb{Z}} \gamma_k \hat{u}_k e^{\frac{2i\pi kx}{L}}.$$

We have the following result:

Proposition 3. *Consider $\mathcal{L}_1$ and and $\mathcal{L}_2$, two weak damping operators defined by*

$$\mathcal{L}_1 = \gamma Id \text{ and } \mathcal{L}_2(u) = \sum_{k\in\mathbb{Z}} \gamma_k \hat{u}_k e^{\frac{2i\pi kx}{L}}.$$

We denote by u (resp. v) the solution of the damped KdV equation with $\mathcal{L}_1$ (resp. $\mathcal{L}_2$) as damping operator. Assume that
– $\gamma_k > 0, \gamma_k = \gamma, |k| \leq N, \gamma_k \leq \gamma, |k| \geq N$
– $\exists \beta > 0/\gamma - \frac{1}{2}|v_x|_\infty \geq \beta > 0,\ \forall t > 0$
Then

$$|w(t)|^2 \leq e^{-\beta t}|w(0)|^2 + \gamma_{N+1}\frac{1 - e^{-\beta t}}{\beta^2}|v(0)|^2$$

where $w = u - v$.

Proof. We have directly

$$\frac{1}{2}\frac{d|w|^2}{dt} + \beta|w|^2 + < (\mathcal{L}_1 - \mathcal{L}_2)(v), w >= 0.$$

Now

$$| < (\mathcal{L}_1 - \mathcal{L}_2)(v), w > | \leq \frac{1}{2\beta}\|\mathcal{L}_1 - \mathcal{L}_2\|^2 + \frac{\beta}{2}|w|^2,$$

here $\|\mathcal{L}_1 - \mathcal{L}_2\|$ denotes the norm of the linear operator $\mathcal{L}_1 - \mathcal{L}_2$ from L^2 to L^2. We have for any $z \in L^2$

$$|(\mathcal{L}_1 - \mathcal{L}_2)(z)|^2 = \sum_{k=N+1}^{+\infty} \gamma_k |\hat{z}_k|^2 \leq \gamma_{N+1}|z|^2.$$

Finally,

$$\frac{d|w|^2}{dt} + \beta|w|^2 \leq \frac{\gamma_{N+1}}{\beta}|v|^2 \leq \frac{\gamma_{N+1}}{\beta}|v(0)|^2,$$

hence the result by using an integration in time. □

3 Numerical Schemes

3.1 Discretization in space

The Damped KdV equation is studied here on the torus, it is then natural to use pseudo-spectral Fourier collocation techniques for the discretization in space; this produces a high accurate discretization and moreover it allows to take advantage of FFT and to make the computations more faster. We shall follow this approach for all the damping we consider except for the local space damping $\mathcal{L}(u) = \chi_{[a,b]}u$. Indeed, since this term is spatially localized, it is very badly localized in frequencies, so the Fourier approach can not be efficient. A way to overcome this drawback while having a high level of accuracy, that can be compared with the spectral one, is to implement finite difference compact schemes [21]. In two words, these schemes consist in approaching a linear operator (differentiation, interpolation) by a rational (instead of polynomial-like) finite differences scheme: let $U = (U_1, \cdots, U_n)^T$ be a vector whose the components are the approximations of a regular function u at (regularly spaced) grid points $x_i = ih$, $i = 1, \cdots, n$. The classical finite difference schemes consists in computing $\mathcal{T}u = f$ at x_i with the matrix-vector product

$$F = TU,$$

where T is the discretization matrix of $\mathcal{T}$n, a derivation or an interpolation operator. The relation $f(x_i) = (TU)_i$ is then satisfied up to a certain order of accuracy. The compact schemes consist in approaching $\mathcal{T}u$ as

$$PF = QU,$$

in such a way the relation $f(x_i) = (P^{-1}QU)_i$ is satisfied at the most possible higher order. The matrix P represents the implicit part of the scheme while Q is the explicit part. We reconsider here the compact schemes introduced by Lele [21]. These schemes are defined with a compact stencil: the implicit part consists of a banded matrix, easy to invert, and thanks to the implicit part, the discretization scheme uses only few points near the boundaries, when the non-periodic case is considered, see [21]. To approach $\frac{\partial u}{\partial x}(x_i)$ we consider the relations

$$u'(x_i) + \alpha(u'(x_{i+1}) + u'(x_{i-1})) + \beta\,(u'(x_{i+2}) + u'(x_{i-2})) = a\frac{u(x_{i+1}) - u(x_{i-1})}{2h} + b\frac{u(x_{i+2}) - u(x_{i-2})}{4h} + c\frac{u(x_{i+3}) - u(x_{i-3})}{8h}. \tag{12}$$

Here h is the spatial step size. Coefficients α, β a, b et c are computed in such a way (12) to be satisfied at a given order.

- Order 10 (error in h^{10}) : $c = 1/75, \beta = 1/20, b = 101/150, \alpha = 1/2, a = 17/12$.
- Ordre 8 (error in h^8) : $\beta = 1/36, b = 25/54, \alpha = 4/9, a = 40/27, c = 0$.
- Order 6 (error in h^6) : $b = 1/9, \alpha = 1/3, a = 14/9, c = 0, \beta = 0$.
- Order 4 (error in h^4) : $b = c = \beta = 0, \alpha = 1/4, a = 3/2$.
- Order 2 (error in h^2) :$a = 1, b = c = \alpha = \beta = 0$.

We use the periodic boundary conditions to close the system. In the same way we define the compact scheme for the third derivative in space as

$$\begin{aligned} u^{(3)}(x_i) + \alpha(u^{(3)}(x_{i+1}) + u^{(3)}(x_{i-1})) + \beta(u^{(3)}(x_{i+2}) + u^{(3)}(x_{i-2})) = \\ a\frac{-2\cdot u(x_{i+1}) + 2\cdot u(x_{i-1}) + u(x_{i+2}) - u(x_{i-2})}{2h^3} \\ +b\frac{-2\cdot u(x_{i+2}) + 2\cdot u(x_{i-2}) + u(x_{i+4}) - u(x_{i-4})}{16h^3} \\ + c\frac{-2\cdot u(x_{i+3}) + 2\cdot u(x_{i-3}) + u(x_{i+6}) - u(x_{i-6})}{54h^3}. \end{aligned} \tag{13}$$

– Order 6 (error in h^6) : $b = 1/9, \alpha = 1/3, a = 14/9, c = 0, \beta = 0$.
– Order 4 (error in h^4) : $b = c = \beta = 0, \alpha = 1/4, a = 3/2$.
– Order 2 (error in h^2) :$a = 1, b = c = \alpha = \beta = 0$.

3.2 Time discretization schemes

3.2.1 Crank Nicolson schemes

Let $\mathcal{D}$ be the differential operator associated to the first derivative in space. The classical Crank-Nicolson scheme writes as

$$\frac{u^{(n+1)} - u^{(n)}}{\Delta t} + \mathcal{L}_\gamma \left(\frac{u^{(n+1)} + u^{(n)}}{2} \right) + \mathcal{D}^3 \left(\frac{u^{(n+1)} + u^{(n)}}{2} \right) + \frac{1}{4} \mathcal{D} \left((u^{(n+1)})^2 + (u^{(n)})^2 \right) = f, \qquad (14)$$

We will use it for the simulations with non time depending damping. In practice it will be implemented using at each time step a Picard fixed point method, other numerical schemes are presented an studied in [3].

3.2.2 Generalized Gear schemes

The Gear scheme is a popular second order semi implicit scheme to solve evolution problems such as parabolic ones, see e.g. [16] and the reference therein for the solution of incompressible Navier-Stokes equations ; it addresses to the approximation of the first derivative in time. Dubois *et al* proposed to adapt it to the numerical computation of fractional derivative, particularly the "half-time" derivative.

Here, we aim at approaching the nonlocal operator $G_t^{1/2} u(t) = \frac{1}{\sqrt{\pi}} \int_0^t \frac{u_t(s)}{\sqrt{t-s}} ds$. In [8], the authors propose the following scheme

$$(G_t^{1/2} u)^n = \sqrt{\frac{3}{2\Delta t}} \cdot \sum_{j=0}^{+\infty} g_{j+1} u^{n-j} = \sqrt{\frac{3}{2\Delta t}} \cdot \sum_{j=0}^{n} g_{n+1-j} u^j,$$

where g_j are the Gear coefficients computed in [7]. Taking the Fourier series of each term we have

$$a_0 \frac{d}{dt} \widehat{u}_k + \sqrt{\nu} \cdot G_t^{1/2} \widehat{u}_k + \underbrace{\left[a_1 \cdot i \cdot \left(\frac{2\pi k}{L} \right) - a_2 \cdot i \cdot \left(\frac{2\pi k}{L} \right)^3 + a_4 \cdot \left(\frac{2\pi k}{L} \right)^2 \right]}_{\text{LT}} \cdot \widehat{u}_k + \underbrace{a_3 \cdot i \cdot \left(\frac{2\pi k}{L} \right)}_{\text{NLT}} \cdot \frac{\widehat{u^2}_k}{2} = 0.$$

We now set $C = \frac{2\pi k}{L}$, $\text{LT} = C \cdot \left(a_1 \cdot i - a_2 \cdot i \cdot C^2 + a_4 \cdot C \right)$ and $\text{NLT} = a_3 \cdot i \cdot C$.
Here $a_0,\ a_1,\ a_2,\ a_3,\ a_4$ and ν are given real numbers. The system to be solved is then:

$$\begin{cases} a_0 \frac{d}{dt} \widehat{u}_k + \sqrt{\nu} \cdot G_t^{1/2} \widehat{u}_k + \text{LT} \cdot \widehat{u}_k + \text{NLT} \cdot \frac{\widehat{u^2}_k}{2} = 0, \\ \widehat{u}_k(x, 0) = \widehat{u}_k(0). \end{cases}$$

We will set for the sequel $U(x,t) = u(x,t) - u_0(x)$, so

$$\begin{cases} a_0 \frac{d}{dt} \widehat{U}_k + \sqrt{\nu} \cdot G_t^{1/2} \widehat{U}_k + \text{LT} \cdot \left(\widehat{U}_k + \widehat{u_0} \right) + \text{NLT} \cdot \frac{\widehat{(U + u_0)^2}_k}{2} = 0, \\ \widehat{U}_k(x, 0) = 0. \end{cases}$$

For simplicity, we consider the following explicit scheme

$$\begin{cases} a_0 \dfrac{\widehat{U}_k^{n+1} - \widehat{U}_k^n}{\Delta t} + \sqrt{\nu} \cdot G_t^{1/2} \widehat{U}_k^{n+1} + \mathrm{LT} \cdot \left(\widehat{U}_k^{n+1} + \widehat{u_0} \right) + \mathrm{NLT} \cdot \dfrac{\widehat{(U^{n+1})^2}_k}{2} = 0, \\ \widehat{U}_k(x,0) = 0. \end{cases}$$

We have $\sqrt{\nu} \cdot G_t^{1/2} \left(\widehat{U}_k^{n+1} \right) = \sqrt{\nu} \cdot \sqrt{\dfrac{3}{2\Delta t}} \cdot \sum_{j=0}^{n+1} g_{n+1-j} U^j = \sqrt{\nu} \cdot \sqrt{\dfrac{3}{2\Delta t}} \cdot \left(g_0 \widehat{U}_k^{n+1} + \sum_{j=0}^{n} g_{n+1-j} U^j \right)$.

Therefore, we obtain

$$\begin{cases} \widehat{U}_k^{n+1} = \left[-\sqrt{\dfrac{3\nu\Delta t}{2}} \cdot \sum_{j=0}^{n} g_{n+1-j} U^j + a_0 \cdot \widehat{U}_k^n - \Delta t \cdot \left(\mathrm{LT} \cdot \widehat{u_0} + \mathrm{NLT} \cdot \dfrac{\widehat{(U^{n+1})^2}_k}{2} \right) \right] / M1, \\ \widehat{U}_k(x,0) = 0. \end{cases}$$

where $M1 = a_0 + \Delta t \cdot \mathrm{LT} + \sqrt{\dfrac{3\nu\Delta t}{2}} \cdot g_0$.

Remark 4. *The Gear scheme proposed here can be generalized to the approximation of general fractional derivatives of order α expanding formally the αth power of the operator scheme expressed with translation operators [10, 18, 19]. We have indeed*

$$G = \frac{1}{\Delta t} \left(\frac{3}{2} I - 2\delta^- + \frac{1}{2} (\delta^-)^2 \right)$$

where δ^- is the time backward translation operator : $\delta^- u^n = u^{n-1}$. Hence

$$(G^\alpha u)^n = \left(\frac{3}{2\Delta t} \right)^\alpha \sum_{j=0}^{+\infty} \sum_{\ell=0}^{j} \left(\frac{4}{3} \right)^j \left(\frac{41}{4} \right)^\ell A_{j+1}^\alpha B_{\ell+1}^j u^{n-j-\ell}.$$

The coefficients A_{j+1}^α and $B_{\ell+1}^j$ being computed recursively by the formula

$$A_{j+1}^\alpha = \frac{j-\alpha-1}{j} A_j^\alpha \text{ and } B_{\ell+1}^k = \frac{\ell-j-1}{\ell} B_\ell^j$$

starting from $A_1^\alpha = 1$ and $B_1^j = 1$. We recover the scheme proposed by Dubois for $\alpha = \frac{1}{2}$ reordering the sum as

$$(G^\alpha u)^n = \left(\frac{3}{2\Delta t} \right)^\alpha \sum_{j=0}^{+\infty} g_{j+1}^\alpha u^{n-j}.$$

4 Numerical results

The numerical results we present here are obtained using Matlab. We will have use of the following notations for the initial data:

$$\begin{aligned} &u_0(x) = S1 = 3\,c\,\mathrm{sech}\left(\sqrt{\frac{c}{2}} (x - pL) \right)^2, \text{ with } c = 1, p = 0.4 \text{ is the soliton,} \\ &u_0(x) = S2 = \chi_{[a,b]} \text{ corresponds to the crennel,} \\ &u_0(x) = S3 = \sin\left(\frac{2\pi x}{L} \right) \text{ is the sine data.} \end{aligned}$$

4.1 The different damping

4.1.1 $\mathcal{L}_\gamma$ damping

In Figure 1, we display (on the left) the time evolution of the L^2-norm of the solution when considering various weak damping operators, the corresponding Γ function is also represented (on the right). The initial data are the same in all cases is soliton-like, say $u_0(x) = 3\,\mathrm{sech}\left(x - 0.4\frac{L}{2}\right)^2 + c$ with c chosen such as u_0 is zero mean. We observe that, of course, the weaker is the damping the slowest the L^2 norm of the solution converges towards 0.

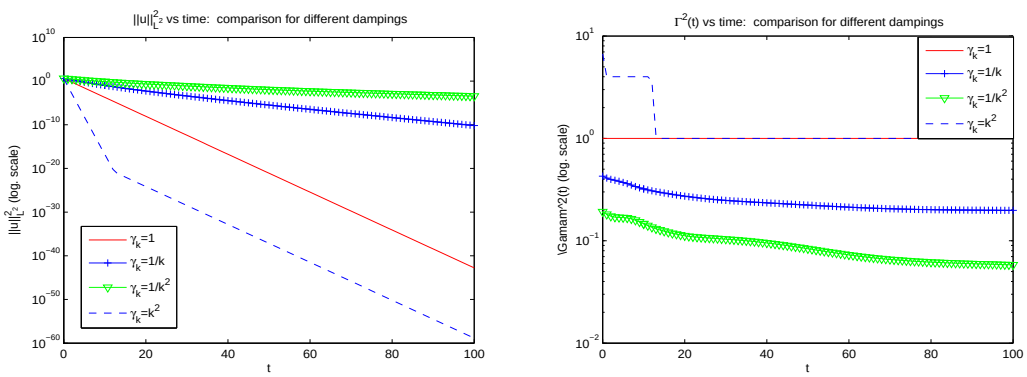

Figure 1: Comparison of L^2-norm of the solution for different damping on $[0, L]$ with $L = 20$ (left) and of $\Gamma^2(t)$ (right).

4.1.2 Local damping in space $\mathcal{L} = \chi_{[a,b]}$

We now represent the evolution of the solution when considering different damping operators localized in space, say of the form $\mathcal{L} = \chi_{[a,b]}$ with $[a, b] \subset [0, L]$. We consider the following situations:
$\mathcal{L} = \chi_{[0,L/4]}$, $\mathcal{L} = \chi_{[0,L/2]}$, $\mathcal{L} = \chi_{[0,3L/2]}$, $\mathcal{L} = \chi_{[0,L]}$.

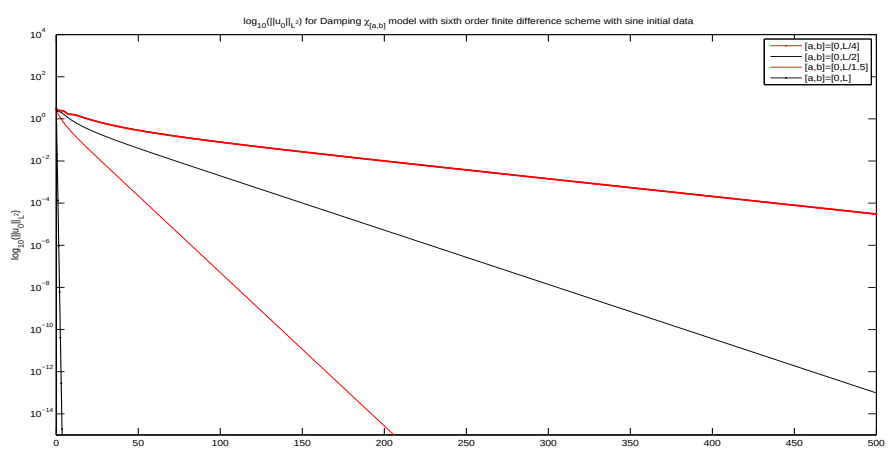

Figure 2: Norm L^2 for the damping $\chi_{[a,b]}$ using a sixth order compact scheme.

We report in Figure 2, the time evolution of the L^2 norm, we note that the damping rate is larger with large values of $b - a$. After a transient time, we see that the L^2 decreases linearly in log. scale, so the

damping is exponential. Similar results are obtained with different initial data. In Figure 3 we compare the time evolution of the L^2 norm of the solution when considering $\mathcal{L} = \chi_{[0,L/2]}$ and various initial data. After a transient time, we note that the rate are the same for each case.

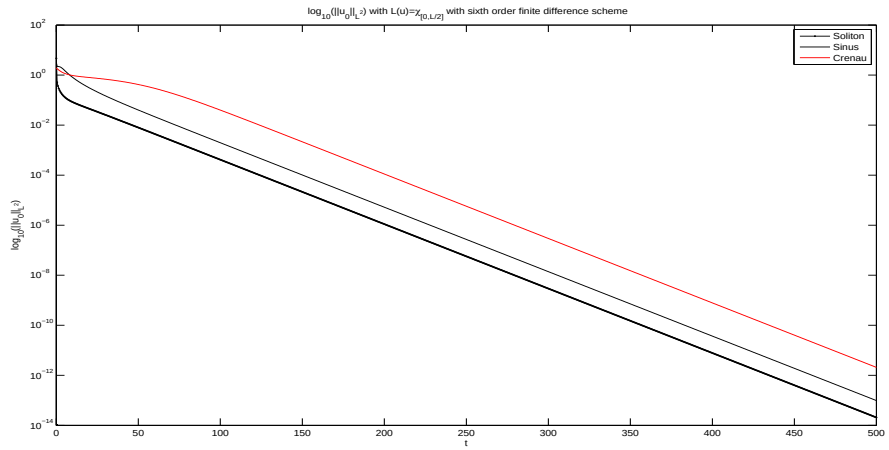

Figure 3: Norm $|u|_{L^2}$ for the damping $\chi_{[0,L/2]}$ using a sixth order compact scheme for initial data: $S1$, $S2 = \chi_{[0.5\cdot L, 0.7\cdot L]}$ et $S3$.

Finally, in Figure 4, we have represented the time evolution of $\Gamma^2(t)$ for different initial data. We observe that, after a transient time, $\Gamma^2(t)$ converge quickly to a constant: this means that the damping rate for large times is the same for all initial data.

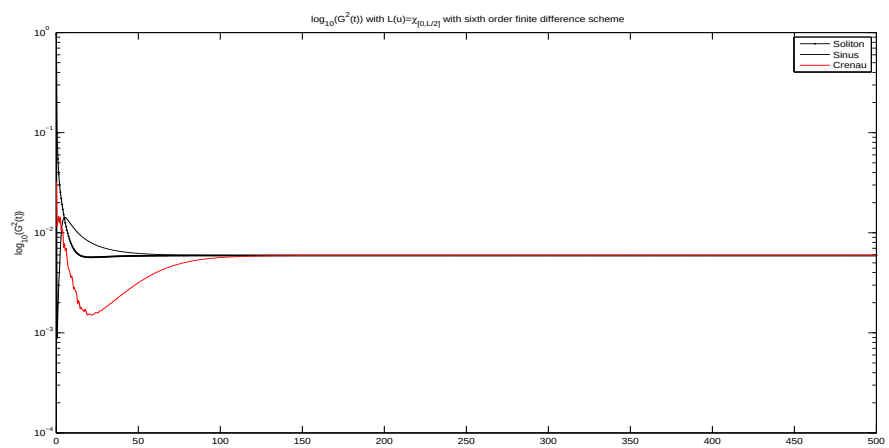

Figure 4: $\Gamma^2(t)$ for the damping $\chi_{[0,L/2]}$ using a sixth order compact scheme for initial data: $S1$, $S2 = \chi_{[0.5\cdot L, 0.7\cdot L]}$ et $S3$.

4.1.3 Nonlocal integral damping

We display hereafter the solution at different times, varying μ and ν. The numerical results agree with whose in [4] (Figure 5).

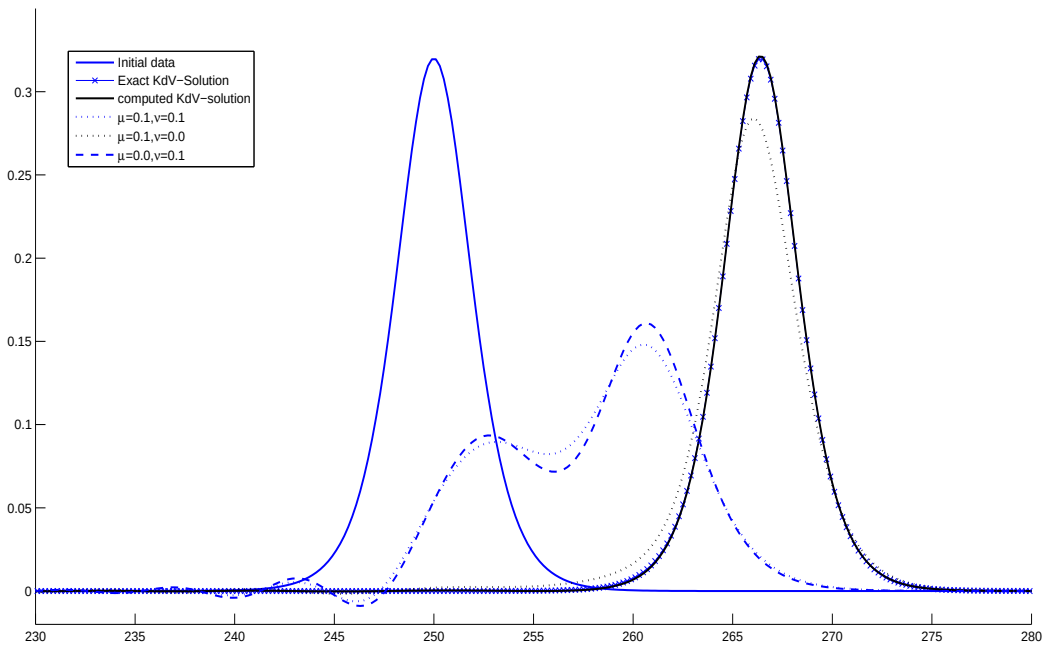

Figure 5: $T = 10, N = 2499, 0 < x < 500, a_0 = 1, a_1 = 1, a_2 = 1, a_3 = 6, a_4 = \mu$.

4.2 Comparison of the damping rates for the different models

In Figures 6 and 7, we compare the long time effect of the different damping using the function $\Gamma(t)$. This approach allows to point out a hierarchy between these different damping models. To this end, we consider the damping operator in its largest generality:

$$\mathcal{L}(u) = \mu\mathcal{L}_\gamma(u) + \sqrt{\nu}\int_0^t \frac{u_t}{\sqrt{t-s}}ds + \omega\chi_{[a,b]}u \tag{15}$$

The case $\nu = \omega = 0$, allows to recover the weak damping when γ_k is bounded and the parabolic damping when $\gamma_k = k^2$, a comparison have been made in Figure 1; when $\nu = \mu = 0$, the nonlocal spatial damping considered for the stabilization is obtained; finally, when $\omega = \mu = 0$, $\nu \neq 0$, $\mathcal{L}$ is the nonlocal damping in time.

To compare the damping effect in L^2 norm of these operators, we distinguish two groups of them

– $\mathcal{L}(u) = \mathcal{L}_\gamma(u)$ or $\mathcal{L}(u) = \chi_{[a,b]}u$
  As seen above, the damping in L^2-norm is exponential in time, after eventually a transient time. For making the comparison coherent, we have scaled the models $\mathcal{L}_\gamma(u)$ in such a way the coefficient associated to the frequency $k = 1$, γ_1 is equal to 1, that is $\mu = \left(\frac{L}{2\pi}\right)^2$; we take $\omega = 1$ since asymptotically, the local spatial damping is to be compare asymptotically with $\mathcal{L}_{\gamma=1} = \chi_{[0,L]}$.

– $\mathcal{L}(u) = -\mu u_{xx} + \sqrt{\nu}\int_0^t \frac{u_t}{\sqrt{t-s}}ds$. Here we have to take into account of the competition between $-\mu u_{xx}$ and $\sqrt{\nu}\int_0^t \frac{u_t}{\sqrt{t-s}}ds$ acording to the values of μ and ν.

Overall, we can range the operators in the following way, by decreasing damping rate

1. $\mathcal{L}(u) = \nu\int_0^t \frac{u_t}{\sqrt{t-s}}ds$
2. $\mathcal{L}(u) = -\mu\partial_x^2 u$
3. $\mathcal{L}(u) = \gamma u$
4. $\mathcal{L}(u) = \gamma u \chi_{[a,b]}$
5. $\mathcal{L}(u) = \mathcal{L}_\gamma(u) = \sum_{k\in Z} \gamma_k \hat{u}_k e^{\frac{2ik\pi x}{L}}$, with $\gamma_k = \frac{1}{1+|k|}$

In Figure 6, we observe a hierarchy between the operators of dissipation through the damping they produce in long time interval, we can distinguish 2 groups, from the most to the less dissipative: first the laplacian-like and the weak operators $\mathcal{L}_\gamma$ with γ bounded, then the damping of type $\chi_{[a,b]}$.

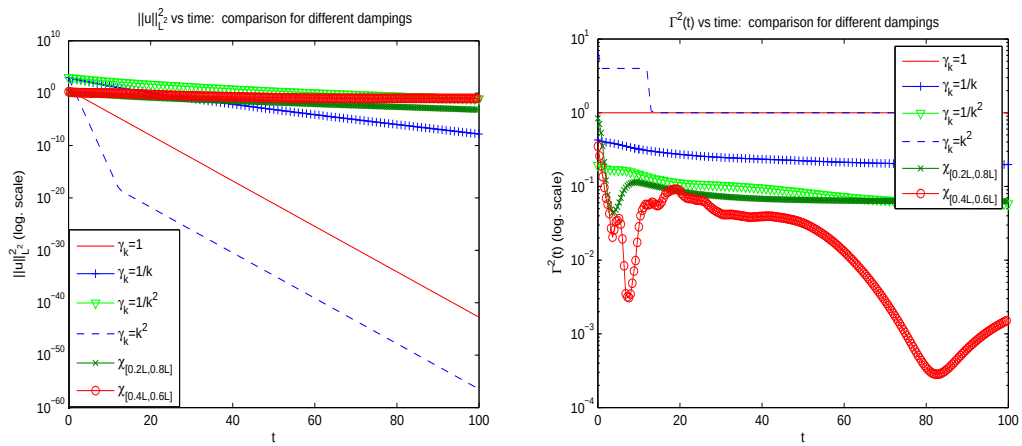

Figure 6: Comparison of the time evolution of L^2-norm (left) and of $\Gamma^2(t)$ (right) for the damping operators $\mathcal{L}_\gamma$ and $\chi_{[a,b]}$ on $[0, L]$ with $L = 20$.

Similar results are obtained starting from different initial data.

In Figure 7, we observe that the damping provided by the nonlocal operator is stronger than that produced by the negative laplacian.

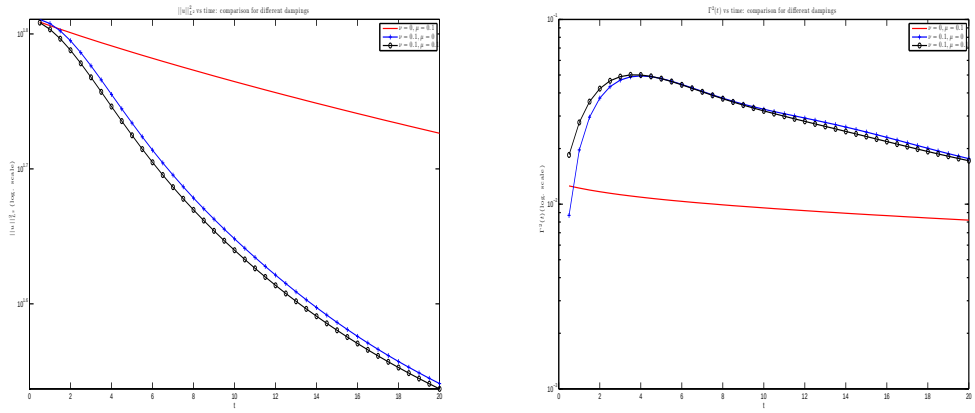

Figure 7: Comparison of the time evolution of L^2-norm (left) and of $\Gamma^2(t)$ (right) for the damping operators $\mathcal{L}(u) = -\mu u_{xx} + \sqrt{\nu}\int_0^t \frac{u_t}{\sqrt{t-s}}ds$ for different ν and μ with $L = 500$.

4.3 Time signal analysis and damping modeling

4.3.1 Time signal analysis

As pointed out in section 2, $\Gamma(t)$ does not belong in $L^2_t(0,+\infty)$. However, it is possible in some cases to find a weight ω such that $G \in L^2_\omega(0,+\infty) = \{v/\int_0^{+\infty} v^2\omega dx < +\infty\}$. In such a case a time signal analysis can be displayed in the orthogonal polynomial basis associated to the scalar product in L^2_ω; for example, if $G(t)$ is at most at polynomial growth, then it belongs in L^2_ω with $\omega = e^{-t}$ so that the time analysis can be done with Laguerre polynomials. This behavior in time was observed for the various damping models, see above.

To display a time signal analysis, we proceed as follows: formally the time signal $\Gamma^2(t)$, is decomposed into the Polynomial Laguerre basis as

$$\Gamma^2(t) = \sum_{k=0}^{+\infty} g_k L_k(t),$$

where L_k is the k-th Laguerre polynomial, defined as the orthogonal sequence with respect to the scalar product $< f, g >= \int_0^{+\infty} fge^{-t}dt$ with $L_0 = 1$. We have then

$$g_k = \frac{\int_0^{+\infty} \Gamma^2(t)L_k(t)e^{-t}dt}{\int_0^{+\infty} L_k^2(t)e^{-t}dt}.$$

Of course, such integral terms can not be computed numerically and they are approached by using Laguerre rule associated to Gauss formula, see [27]. To post-treat sampled values of $\Gamma^2(t)$ $(t_i, \Gamma^2(t_i)), i = 1, \cdots, n$ produced by a numerical solver of Damped KdV equation, we first fit the discrete time t_i to Gauss points of the Laguerre rule formula, $\xi_j, j = 0, \cdots, m$, with $m << n$, the weight

are noted w_j; then we use as data $(\xi_j, \Gamma^2(\xi_j)$ to make signal time analysis and synthesis:

$$g_k^n = \frac{\displaystyle\sum_{j=0}^{m} \Gamma^2(\xi_j) L_k(\xi_j) w_j}{\displaystyle\sum_{j=0}^{m} L_k^2(\xi_j) w_j},$$

so that

$$\Pi_n(\Gamma^2)(t) = \sum_{k=0}^{m} g_k^n L_k(t),$$

is the interpolation polynomial of Γ^2 at the points $\xi_j,\ j = 0, \cdots, m$.
We display hereafter in Figures (8) and (9) the time signal analysis and synthesis of $\Gamma^2(t)$ for the damping operators considered above.

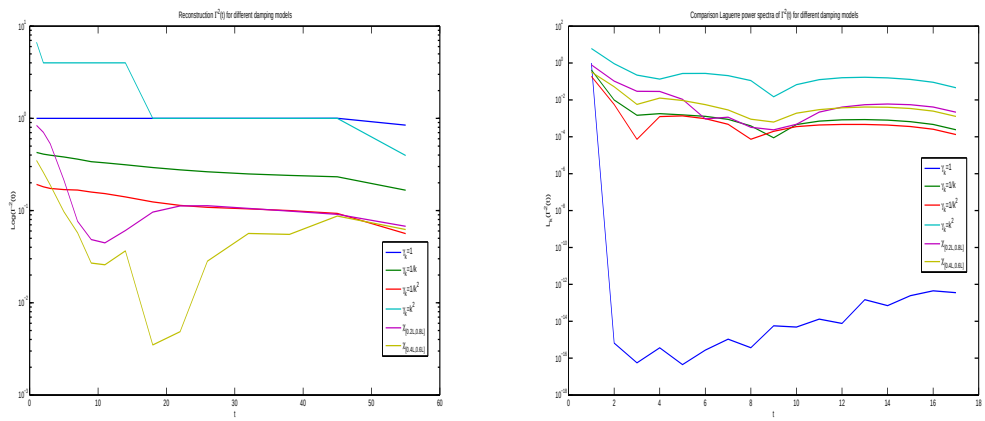

Figure 8: Comparison of the power spectrum of $\Gamma^2(t)$ for the damping operators $\mathcal{L}_\gamma$ and $\chi_{[a,b]}$ on $[0, L]$ with $L = 20$ (left), reconstruction of the signal (right)

4.3.2 Reconstruction of the damping operator with sample data

We now describe a way to build *a posteriori* the damping operator $\mathcal{L}$ in the cases of a local damping in space, i.e. when $\mathcal{L} = \chi_{[a,b]}$, and of a weak damping.
The key is the knowledge of numerical values of u at discrete times $t_m,\ m = 1, \cdots M$; these values can be computed by a numerical code or measured experimentally. Indeed, with theses data we are able to compute approximate values of $\Gamma^2(t_m)$: by integrating the differential equation

$$\frac{1}{2}\frac{d|u|^2}{dt} + \Gamma^2(t)|u|^2 = 0,$$

between t_m and t_{m+1} with, e.g., the semi-implicit scheme

$$\frac{|u(t_{m+1})|^2 - |u(t_m)|^2}{\Delta t} + \Gamma^2(t_{m+1})\frac{1}{2}(|u(t_{m+1})|^2 + |u(t_m)|^2),$$

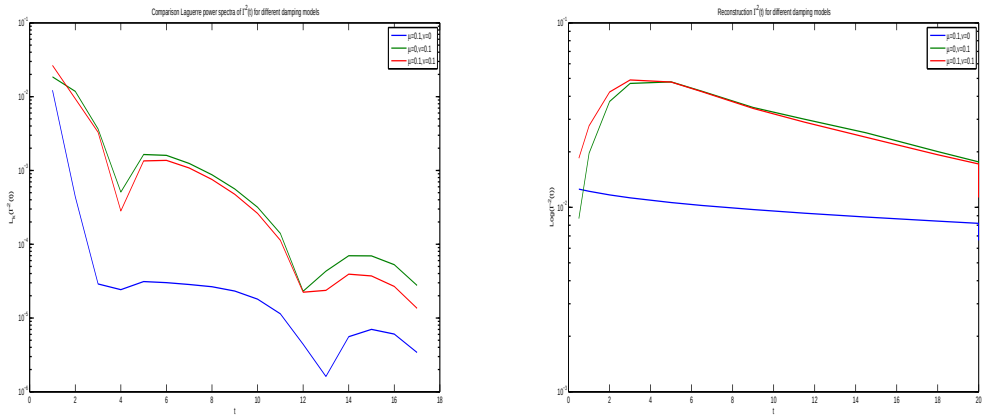

Figure 9: Comparison of the power spectrum of $\Gamma^2(t)$ for the damping operators $\mathcal{L}(u) = -\mu u_{xx} + \sqrt{\nu}\int_0^t \frac{u_t}{\sqrt{t-s}}ds$ for different ν and μ with $L = 500$ (left), reconstruction of the signal (right)

and we get

$$\Gamma^2(t_{m+1}) \simeq \frac{|u(t_m)|^2 - |u(t_{m+1})|^2}{\Delta t(|u(t_{m+1})|^2 + |u(t_m)|^2)}.$$

We first consider the case of the local damping in space $\mathcal{L} = \chi_{[a,b]}$. Let x_i be the (regularly spaced) grid points and ℓ_i the vector defined by

$$\ell_i = \begin{cases} 1 & \text{if } x_i \in [a,b], \\ 0 & \text{otherwise.} \end{cases}$$

The computed values of $\Gamma^2(t_m)$ at discrete times t_m are the numbers

$$\Gamma^2(t_m) = \frac{\sum_{i=1}^{N} \ell_i u_i^2 h}{\sum_{i=1}^{N} u_i^2 h},$$

hence, we look to positive real numbers γ_i solution of the constraint least square problem

$$\operatorname*{Inf}_{\gamma_i \geq 0} \sum_{m=0}^{M} \left(\frac{\sum_{i=1}^{N} \gamma_i (u_i^m)^2}{\sum_{i=1}^{N} (u_i^m)^2} - \Gamma^2(t_m) \right)^2.$$

This minimization problem will be solved numerically using the Matlab® function `fmincon`.
In the case of the weak damping operator $\mathcal{L}(u) = \sum_{k\in\mathbb{Z}} \gamma_k \hat{u}_k e^{\frac{2i\pi k x}{L}}$ we proceed as follows: given the

samples $\Gamma(t_m), m = 0, \cdots, M$ we can write

$$\Gamma^2(t) = \frac{\sum_{k\in\mathbb{Z}} \gamma_k |\hat{u}_k(t)|^2}{\sum_{k\in\mathbb{Z}} |\hat{u}_k(t)|^2}.$$

We want to find the coefficients γ_k that fit these relations. Of course we'll look to a finite number of them, so that satisfying at the least square sense the relation

$$\sum_{m=0}^{M} \left(\sum_{|k|\leq N} \gamma_k | \frac{\hat{u}_k(t_m)|^2}{\sum_{|k|\leq N} |\hat{u}_k(t_m)|^2} - \Gamma^2(t_m) \right)^2$$

with the constraints

$$\gamma_k > 0.$$

In summary the sequence γ_k solves the problem

$$\operatorname*{Inf}_{\gamma_k \geq 0} \sum_{m=0}^{M} \left(\sum_{|k|\leq N} \gamma_k \frac{|\hat{u}_k(t_m)|^2}{\sum_{|k|\leq N} |\hat{u}_k(t_m)|^2} - \Gamma^2(t_m) \right). \tag{16}$$

We also solve this problem using the Matlab's function `fmincon`.

The results we give hereafter concern two situations

– Linear KdV equation

$$u_t + \mathcal{L}(u) + u_{xxx} = 0.$$

Here the frequencies are not melted by a nonlinear term, and the damping is active independently frequency by frequency.

– the nonlinear KdV

$$u_t + \mathcal{L}(u) + u_{xxx} + uu_x = 0.$$

Here the nonlinear term melts the frequencies

In both the cases we have

$$\frac{1}{2}\frac{d|u|^2}{dt} + < \mathcal{L}(u), u >= 0.$$

4.3.3 Linear KdV

We start from a soliton-like data $u(x,0) = 2c_1 \text{sech}(\sqrt{c_1}(x - p_1 L))^2$ with $c_1 = 0.16,\ p_1 = 0.5$; here $L = 20$, $N = 2^7$ and $\Delta t = 0.01$. The original operator is $\mathcal{L}_\gamma$ with $\gamma_k = \gamma = 2.7$.

In Figure 10, we observe that the operator is rebuild in a relatively satisfactory way.

Now, we take the same data as before, but here $\gamma_k = \dfrac{1}{(1+|k|)^2}$.

We observe in Figure 11 that the reconstruction is correct only for the low frequencies. This is due to the ill-conditioning of the problem.

4.3.4 Nonlinear KdV

First we give numerical results concerning the reconstruction of the local damping in space $\mathcal{L} = \chi_{[0.4L, 0.6L]}$.

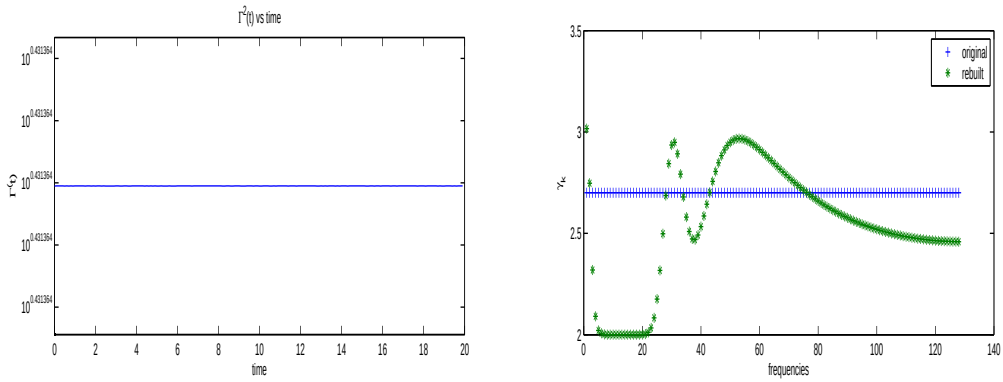

Figure 10: $\Gamma^2(t)$ (left), comparison of the original and the rebuilt coefficients γ_k (right)

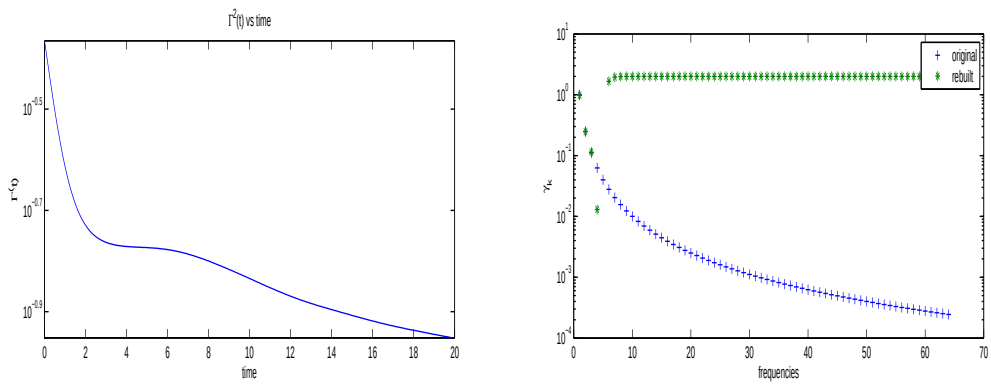

Figure 11: $\Gamma^2(t)$ (left), comparison of the original and the rebuilt coefficients $\gamma_k = \dfrac{1}{(|k|+1)^2}$ (right)

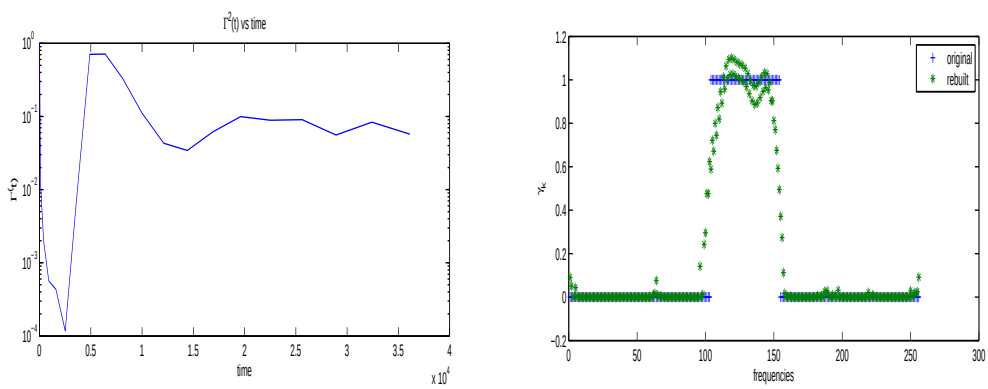

Figure 12: $\Gamma^2(t)$ (left), comparison of the original and the rebuilt coefficients $\mathcal{L} = \chi_{[0.4L,0.6L]}$ (right)

In Figure 12, the result obtained is encouraging: the reconstruction of $\mathcal{L}$ is rather satisfactory. Figure 13 represents the reconstruction of a weak damping operator.
We point out that this numerical recovering of the damping operator is a first step and improvement will be considered in further works. The technique we used for rebuilding the damping operator is the same in the two situations we have considered. However, if the results are encouraging when considering the local damping in space, it is not the case for the weak damping operator.

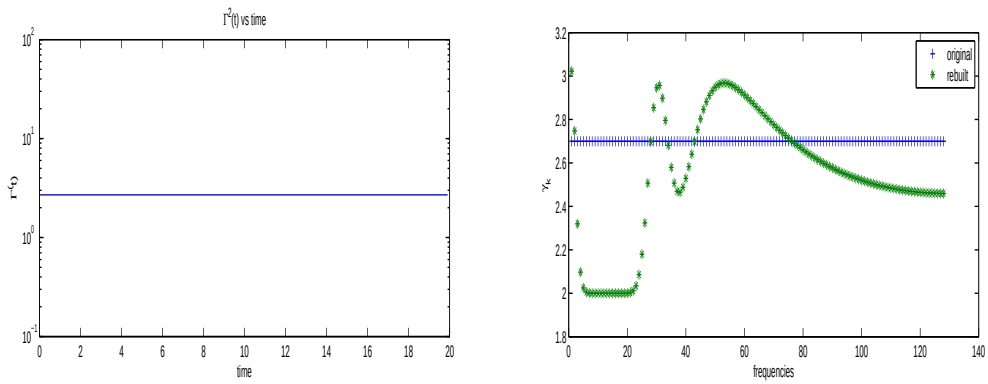

Figure 13: $\Gamma^2(t)$ (left), comparison of the original and the rebuilt coefficients γ_k (right)

Indeed, the matrix $A_{m,k} = \dfrac{|\hat{u}_k(t_m)|^2}{\sum_{|j|\leq N} |\hat{u}_j(t_m)|^2}$ is ill-conditioned so, for instance, regularization techniques should be considered together with the minimization solver. In a larger way, the reconstruction of $\mathcal{L}$ should be done using recent techniques for the solution of inverse problems, see, e.g., [17].

5 Concluding remarks

The function $\Gamma(t)$ seems to be an interesting way to compare the large time effect of various damping models for KdV equations and more widely for damped conservative equations of type

$$u_t + \mathcal{L}(u) + F(u) = 0 \tag{17}$$

with $< F(u), u >= 0$.
The knowledge of samplings of the solution can be exploited in a encouraging way to rebuild a parametrized damping operator. Of course, this last approach as presented here is only a first step and improvements should be obtained using techniques coming from inverse problem area such as those presented recently in [17], particularly for coupling regularization techniques with the solution of ill-conditioned constrained quadratic minimization problems. This is addressed to further developments.

References

[1] J. L. Bona, M. Chen, and J.-C. Saut, Boussinesq equations and other systems for small- amplitude long waves in nonlinear dispersive media I: Derivation and the linear theory, J. Nonlinear Sci., 12 (2002), pp. 283–318.

[2] M. Cabral and R. Rosa, Chaos for a damped and forced KdV equation, Phys. D, **192** (2004), 265–278.

[3] J.-P. Chehab and G. Sadaka, Numerical study of a family of damped KdV equations, CPAA, Volume 12, Number 1, (2013), pp 519 – 546.

[4] M. Chen, S. Dumont, L. Dupaigne and O. Goubet, Decay of solutions to a water wave model with nonlocal viscous dispersive term, discrete and continuous dynamical systems, Volume 27, Number 4, August 2010 pp. 1473-1492.

[5] F. Dias, D. Dutykh, Viscous potentiel free-surface flows in a fluid layer of finite depth, C.R. Math. Acad. Sci. Paris, 345 (2007), pp. 113-118.

[6] D. Dutykh, Visco-potential free-surface flows and long wave modeling. European Journal of Mechanics B/Fluids, 28(3), 430 - 443, 2009

[7] F. Dubois, *http://www.math.u-psud.fr/∼ fdubois/travaux/evolution/marrakech01/semidif4/semidif4.juin01.f*

[8] F. Dubois, A. Galucio et N. Point, *Introduction à la dérivation fractionnaire ; théorie et applications*, Ref AF510, Techniques de l'ingénieur, april 2010.

[9] F. Dubois, A. Galucio et N. Point, The G^{α}-scheme for approximation of fractional derivatives: application to the dynamics of dissipative systems. (English summary) J. Vib. Control 14 (2008), no. 9-10, 1597–1605

[10] S. Dumont, J.-B. Duval, Numerical investigation of asymptotical properties of solutions to models for waterwaves with non local viscosity, S. Dumont, J.-B. Duval, International Journal of Numerical Analysis and Modeling, to appear (2012).

[11] D. Dutykh, *Modélisation mathématique des Tsunamis*, Thèse de doctorat, ENS Cachan, 2007.

[12] J-M. Ghidaglia, *Weakly damped forced Korteweg-de Vries equations behave as a finite dimensional dynamical system in the long time*, J. Diff. Eq., 74, pp 369-390, (1988).

[13] J-M. Ghidaglia, *A note on the strong convergence towards attractors for damped forced KdV equations*, J. Diff. Eq. **110**, 356-359, (1994).

[14] O. Goubet, *Asymptotic smoothing effect for weakly damped forced Korteweg-de Vries equations*, Discrete Contin. Dynam. Systems **6** (2000), no. 3, 625–644.

[15] O. Goubet, R. Rosa *Asymptotic smoothing and the global attractor of a weakly damped KdV equation on the real line* , J. Differential Equations **185** (2002), no. 1, 25–53.

[16] J. L. Guermond, P. Minev, J. Shen, An Overview of Projection Methods for Incompressible Flows. Comput. Methods Appl. Mech. Eng. 195:6011-6045

[17] J. Guerrero, M. Raydan, M. Rojas, A hybrid optimization method for large-scale non-negative full regularization in image restoration, Inverse Problems in Science ad Engineering, to appear (2012)

[18] C. Hirsch, *Numerical Computation of Internal and External Flows , The Fundamentals of Computational Fluid Dynamics*, Butterworth-Heinemann, 2007

[19] C. Jordan, *Calculus of Finite Differences*, 3rd ed. New York: Chelsea, 1965.

[20] C. Laurent, L. Rosier, B-Y Zhang, Control stabilization of the Korterweg-De-Vries equation in a periodic domain, Comm. PDE, 35: 707-744, 2010.

[21] Lele, S. K. (1992). Compact finite difference schemes with spectral-like resolution. J. Comput. Phys. 103, 16-42.

[22] A. Miranville and R. Temam, Mathematical Modeling in Continuum Mechanics, Cambridge University Press, 2005

[23] E. Ott and R.N. Sudan, Nonlinear theory of ion acoustic wave with Landau damping, The Physics of fluids, Vol 12, N 11, 1969.

[24] E. Ott and R.N. Sudan, Damping of solitary waves, The Physics of fluids, Vol 13, N 6, 1970.

[25] A. Pazoto, L. Rosier, Uniform stabilization in weighted Sobolev spaces for the KdV equation posed on the half-space, DCDS-B, Vol. 14, No. 4, Nov. 2010, 1511–1535

[26] G. Sadaka, *Etude mathématique et numérique d'équations d'ondes aquatiques amorties*, thèse de doctorat, Université de Picardie Jules Verne, November 2011.

[27] Lloyd N. Trefethen, Spectral Methods in MATLAB, SIAM, Philadelphia, 2000